ELSEVIER

Journal of Contaminant Hydrology 47 (2001) 29–51

JOURNAL OF Contaminant Hydrology

www.elsevier.com/locate/jconhyd

Analysis of field observations of tracer transport in a fractured till

Georg Kosakowski, Brian Berkowitz *, Harvey Scher

Department of Environmental Sciences and Energy Research, Weizmann Institute of Science, Rehovot 76100, Israel

Received 16 February 2000; received in revised form 21 July 2000; accepted 29 August 2000

Abstract

We analyze a set of observations from a recently published, field-scale tracer test in a fractured till. These observations demonstrate a dominant, underlying non-Fickian behavior, which cannot be quantified using traditional modeling approaches. We use a continuous time random walk (CTRW) approach which thoroughly accounts for the measurements, and which is based on a physical picture of contaminant motion that is consistent with the geometric and hydraulic characterization of the fractured formation. We also incorporate convolution techniques in the CTRW theory, to consider transport between different regions containing distinct heterogeneity patterns. These results enhance the possibility that limitations in predicting non-Fickian modes of contaminant migration can be overcome.

Keywords: Fractured aquifer; Contaminant transport; Stochastic theory; Random walk; Tracer test

1. Introduction

Fractured aquifers are highly complex systems. Within them, groundwater movement is influenced by several superposing factors, which lead to highly variable velocity fields. Controlling factors include small- and large-scale roughness of the fracture walls, presence of fracture filling material, variable fracture network geometry, and interaction with the rock matrix. A principal challenge is to describe the movement of chemicals in such domains. Realistic quantification of this movement is complicated by the uncer-

* Corresponding author. Fax: +972-8-934-4124.

E-mail addresses: g.kosakowski@gmx.net (G. Kosakowski), brian.berkowitz@weizmann.ac.il (B. Berkowitz), harvey.scher@weizmann.ac.il (H. Scher).

0169-7722/01/$ - see front matter
PII: S0169-7722(00)00140-6

tainty in characterization of aquifer properties. As a consequence, modeling approaches which describe the important features of the problem with a minimum of information are needed. In this paper, we focus on the movement of conservative chemicals in saturated fractured aquifers.

In spite of its many limitations, as frequently discussed in the literature (e.g., Adams and Gelhar, 1992; Fitts, 1996; Eggleston and Rojstaczer, 1998), the advection–dispersion equation (ADE) is still used often for the characterization of large-scale tracer movement in fractured formations. Application of the ADE is based on the assumptions that the center of mass of the tracer plume moves with the average fluid velocity, and that dispersion behaves macroscopically as a Fickian diffusive process, with the dispersivity being assumed constant in space and time. Throughout this paper, we shall refer to these assumptions as "Fickian transport assumptions". Although the ADE describes tracer movement for ideal systems, the literature is full of examples demonstrating that the ADE fails to describe tracer transport even in "homogeneous" systems. This is evidently because heterogeneities, which cannot be ignored, occur at all scales and not only on larger scales.

Another approach is to treat the complex geometry of an interconnected fracture system by use of a discrete fracture network (for an extensive overview see, e.g., Chap. 7.2 of Sahimi, 1995). Fractures are modeled as simple planes or discs, which form an interconnected network in space. Flow is described by the Reynolds equation (local cubic law) and contaminant transport is analyzed by use of either direct solution of the transport equation or by use of a particle tracking method. Although discrete fracture models (DFMs) have been applied successfully in specific instances (see, e.g., in National Research Council, 1996), the major disadvantage with this approach is that a full description of the fracture geometry, or at least a good knowledge of the fracture statistics, is needed.

Of course, many alternative modeling approaches exist, including stochastic continuum, double continuum, "discontinuum", and various other hybrid models (National Research Council, 1996). These models have been applied with varying degrees of success; the drawbacks are that their application usually requires large spatial scales and high fracture density, a large number of fitting parameters, and/or a "leap of faith" in order to justify them physically. More importantly, these approaches are often unable to capture even the general measured transport patterns; we suggest that this is because (in addition to the drawbacks just listed) the approaches assume, either implicitly or explicitly, underlying Fickian transport assumptions.

A more general approach to quantifying transport — one that does not rely on Fickian transport assumptions — is based on continuous time random walk (CTRW) theory. It was first applied to electron movement in disordered semiconductors (e.g., Scher and Lax, 1973a,b). In the context of geological materials, CTRW theory was developed and applied to numerical studies of transport in random fracture networks (Berkowitz and Scher, 1997, 1998), and to modeling tracer transport in laboratory flow cells containing porous media (Hatano and Hatano, 1998; Berkowitz et al., 2000). We have recently demonstrated (Berkowitz and Scher, 2000) how the CTRW framework accounts for a very wide range of non-Fickian and Fickian transport behaviors, and how the ADE can be derived from it under specific, well-defined conditions.

In this contribution, we demonstrate application of the CTRW approach on previously published measurements from a natural gradient tracer test, performed in a large, isolated block of fractured till (Sidle et al., 1998). Field measurements of this nature are rare, and the data set examined here is therefore rather unique. In Section 2, we provide a brief summary of the geology, experiment set-up and the results of the hydraulic and tracer tests. We then present aspects of the CTRW theory, and apply it to analyze the tracer test data. These results are compared to those obtained from conventional quantification approaches. In contrast to these other approaches, it is demonstrated that the CTRW thoroughly accounts for the measurements. We further develop the CTRW theory, using convolution techniques, to consider transport between different regions containing distinct heterogeneity patterns. The paper concludes with a discussion of applications of the CTRW theory, and its role in predicting non-Fickian modes of contaminant migration.

2. Description of the field experiment

We consider a natural gradient tracer test in a fractured till. A detailed description of the site and the tracer test can be found in Sidle et al. (1998), while the geometry of the fracture system is described in Klint and Fredericia (1995). Here, we summarize the important features in the context of our present analysis.

The study area is located in Ringe on the isle of Funen in Denmark, in an abandoned creosote factory. The till is of glacial origin and is heavily fractured. The matrix permeability of the till is low and therefore, water flow is attributed mainly to the fractures. Superficially at least, one can divide the entire system into different horizontal layers formed by the intersection of two main nearly vertical fracture systems. The uppermost layer between ground level and 1.5 m, in addition to being fractured, is heavily perturbed by wormholes. From 0.8 to 2.0-m depth, polygonal columns with a diameter of between 0.4 and 0.5 m are formed by desiccation fractures. The spacing between the major desiccation fractures increases rapidly below 2.4 m. The till contains glaciotectonic fractures 1.5 m below ground level. Below 2.0 m, the glaciotectonic fractures have a spacing between 0.3 and 0.4 m. However, as noted by Sidle et al. (1998) and Broholm et al. (2000), it is important to emphasize that variation in the hydraulic properties of these layers is unknown. In particular, lack of information on fracture connectivity and on hydraulic properties of individual fractures, are major sources of uncertainty in quantifying fluid flow and tracer transport. Fig. 1 shows the experimental setup. A block of till was excavated, and three horizontal multiple-port samplers were installed at depths of 2.5 and 4.0 m. Each sampler contained five screened sections, but due to failures in the packers and crossflow between neighboring sections, only 13 of the 30 samplers could be used. An infiltration basis was excavated to a depth of 0.8 m and filled with gravel to a depth of 0.3 m below the natural ground surface. The water level during infiltration was 0.4 m below ground surface. The transport distances from the top of the infiltration basin to the sampling depth are 2.1 and 3.6 m, respectively. Hydraulic tests were performed to estimate for each sampler the

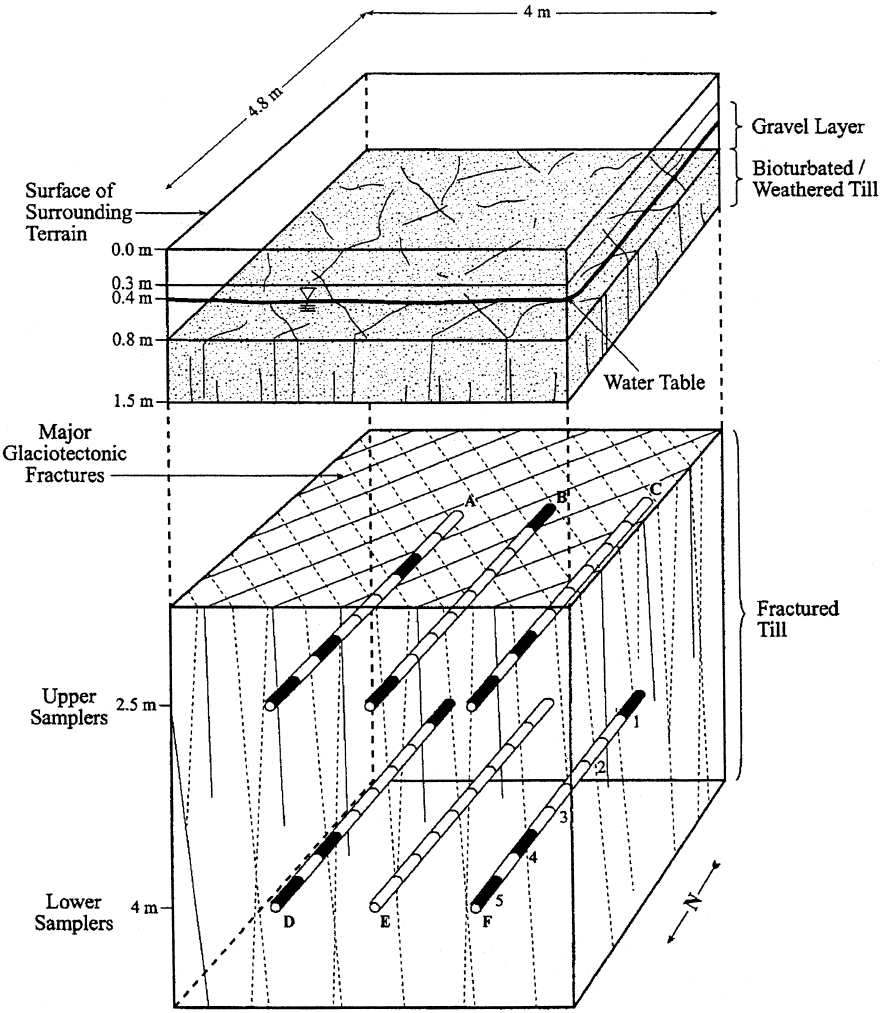

Fig. 1. Schematic illustration of the experimental set-up, including the infiltration basin and the system of horizontal samplers. Also shown are the approximate locations of the two main vertical fracture systems (from Sidle et al., 1998).

hydraulic conductivities, the flow rates and the influence of the excavation of fracture openings on the sampler. The overall hydraulic conductivities were higher for the 2.5-m depth (5.81×10^{-5} ms^{-1}) than for the 4.0-m depth (8.00×10^{-6} ms^{-1}). This can be related to the generally increasing fracture spacing with depth.

The tracer test was initiated with infiltration of municipal water. After steady state flow conditions were established, a solution of ~ 490 mg l^{-1} Cl^{-} was infiltrated for 7 days. During this 7-day period, water samples were collected at lognormal time intervals.

Breakthrough curves for the different sampling locations are shown in Fig. 2. There is very significant temporal and spatial variability in and among the breakthrough curves. The 50% arrival times for the relative concentration (i.e., $C/C_0 = 0.5$, where C_0 is the inlet concentration) ranged between 5.0 and 35.4 h in the upper section, and between 10.7 and 69.2 h in the lower section. In the time scale of the experiment, no curve reaches the maximum input concentration, and most curves reach concentrations between 0.8 and 1.0 (upper curves) and 0.4 and 0.8 (lower curves). All curves show strong fluctuations in the concentration with time, with the concentration in some curves even decreasing systematically at greater times. Some of the fluctuations in the curves appear to be systematic, due to the experimental procedure. For example, nearly all curves show a small decrease in concentration after 1 day. This result can be attributed to technical problems in maintaining a constant inflow concentration (Sidle et al., 1998).

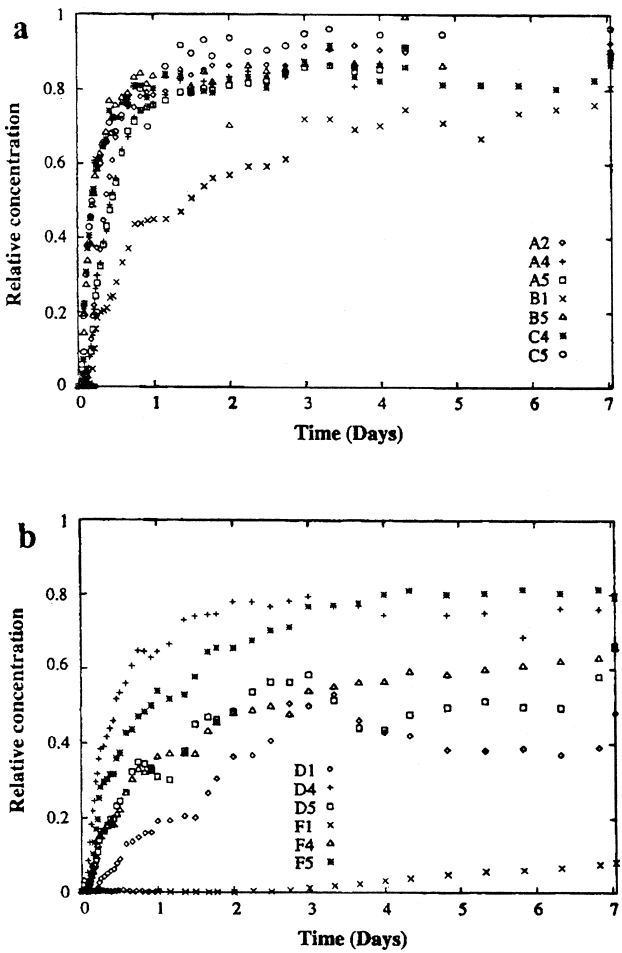

Fig. 2. Measured chloride breakthrough data for (a) seven screened samplers at the 2.5-m depth, and (b) six screened samplers at the 4-m depth (from Sidle et al., 1998).

The temporal fluctuations and the spatial variability of the breakthrough curves are caused by the irregularity of the flow field. At the scale of single fractures, the flow field is controlled by the geometry, the surface roughness of fracture walls, and the variability in fracture aperture and contact areas; these features lead to channeled flow and to an irregular velocity field on a small-scale. An overlying effect, on a larger scale, is a function of the fracture connectivity. Tracer transport can of course also be affected by diffusive interaction with the host rock matrix.

3. Modeling approaches

3.1. Basic conceptual pictures

The measured breakthrough curves shown in Fig. 2 were analyzed by Sidle et al. (1998) using two "classical" modeling approaches. They attempted to fit the measurements with (1) an equivalent porous medium (EPM) model, using the (one-dimensional) ADE, and (2) a DFM based on a parallel fracture conceptualization.

The EPM approach uses a one-dimensional solution of the ADE (Ogata and Banks, 1961). By fitting the number of displaced pore volumes and the Peclet number to the measurements, the pore water velocity u and the longitudinal dispersion D can be determined. The values of water velocity and dispersivity estimated by Sidle et al. (1998) for the various breakthrough curves varied over more than one order of magnitude. Significantly, the EPM approach was unable to capture the full evolution of the measured breakthrough curves (see Section 4). The lack of homogeneity in the flow domain, at least at the scale of the measurements, essentially invalidates the use of this conceptualization.

Use of the DFM, on the other hand, assumes advective transport in the fractures, with diffusion into and within the host matrix. Then, the fracture network (which in reality appears to consist of two main intersecting fracture sets, with variable fracture spacing, as well as several smaller fracture sets connected on a smaller scale) is conceptualized as a set of parallel (unconnected), planar fractures, with flow described by the cubic law. With this approach, Sidle et al. (1998) determined reasonable combinations of the fracture aperture $2b$ and the fracture spacing B which satisfied both the hydraulic and the transport measurements. Notwithstanding the apparent flexibility in fitting such a model to the data, it is significant that, like the EPM model, the DFM was unable to capture the full evolution of the measured breakthrough curves (see Section 4). Also, the estimated water velocity, fracture aperture, and fracture spacing values varied widely for the various breakthrough curves.

Our analysis is motivated by the uniqueness of the field experiment, the high resolution of the data set, the limitations of the EPM and DFM approaches to fit the measured breakthrough curves, and indeed, the characteristic, non-Fickian nature of the transport reflected in these breakthrough curves. We introduce (Section 3.2) a different approach to quantifying tracer transport — one which fully characterizes non-Fickian transport — and demonstrate its application on these same measured breakthrough curves (Section 4).

3.2. CTRW theory and the first passage time distribution (FPTD)

The early and late arrival time behavior displayed in the breakthrough curves shown in Fig. 2, and their asymmetry, are typical of non-Fickian transport. We have shown that a modeling approach based on CTRW theory accounts very well for this type of transport. Examples are tracer migration in numerical simulations in fracture networks (Berkowitz and Scher, 1997, 1998), in a large-scale field experiment in a heterogeneous aquifer (Berkowitz and Scher, 1998) and in laboratory-scale heterogeneous porous media (Berkowitz et al., 2000). The CTRW is based on a physical picture of contaminant motion, which is consistent with the geometric and hydraulic characterization of the fractured till.

The formalism of the CTRW approach is well-documented (Scher and Lax, 1973a,b; Scher and Montroll, 1975; Berkowitz and Scher, 1995, 1998, 2000), therefore, we only summarize the main ideas that are related directly to the following analysis.

Contaminant migration in a strongly varying velocity field can be envisioned as particles executing a series of steps, or transitions, between locales where the velocity changes. The transport is controlled by the coherence lengths of the velocity field and by the scattering among different velocity values. The sporadic interaction of particles in high and moderate velocity paths with low velocity regions often leads to non-Fickian transport behaviors. Non-Fickian transport can arise if the encounter–range relationship between particles and the velocities produces a wide spread of different sequences in the flow paths of the migrating particles.

In a single realization of the medium, the contaminant motion (outlined above) can be described by the "master equation" (Oppenheim et al., 1977; Shlesinger, 1996)

$$\frac{\partial C(\mathbf{s},t)}{\partial t} = -C(\mathbf{s},t)\sum_{\mathbf{s}'} w(\mathbf{s},\mathbf{s}') + \sum_{\mathbf{s}'} w(\mathbf{s}',\mathbf{s})\,C(\mathbf{s}',t) \tag{1}$$

where $C(\mathbf{s}, t)$ represents the particle concentration at point $\mathbf{s}$ and time t and $w(\mathbf{s}, \mathbf{s}')$ is the local transition rate from $\mathbf{s}$ to $\mathbf{s}'$. The basic transport Eq. (1) is valid at any time and (one-, two- or three-dimensional) space scale. The transition rates describe the effects of the velocity field on the particle motion; in Eq. (1) there is no separation of these effects into advective, diffusive and dispersive features. The transitions in the fracture system include both those due to rough-walled large fractures and those due to fracture intersections, as well as migration into and out of the host rock matrix. In relatively homogeneous regions, the $C(\mathbf{s}, t)$ will be slowly varying over some length scale s_0 and Eq. (1) in this region can be reduced to the familiar ADE equation (Berkowitz and Scher, 2000).

The ensemble average of Eq. (1) can be shown (Klafter and Silbey, 1980) to be of the form

$$\frac{\partial P(\mathbf{s},t)}{\partial t} = -\sum_{\mathbf{s}'}\int_0^t \phi(\mathbf{s}'-\mathbf{s},t-t')\,P(\mathbf{s},t')\,\mathrm{d}t' + \sum_{\mathbf{s}'}\int_0^t \phi(\mathbf{s}'-\mathbf{s},t-t')\,P(\mathbf{s}',t')\,\mathrm{d}t' \tag{2}$$

where $P(\mathbf{s}, t)$ is the normalized (relative) concentration. The ensemble-averaged transition rates $\psi(\mathbf{s}, t)$ (defined below) and $\phi(\mathbf{s}, t)$ are related through their Laplace

transforms $\tilde{\psi}(\mathbf{s}, u)$ and $\tilde{\phi}(\mathbf{s}, u)$ (where u is the Laplace variable), with $\tilde{\phi}(\mathbf{s}, u) = [u\tilde{\psi}(\mathbf{s}, u)]/[1\text{-}\tilde{\psi}(u)]$ and $\psi(t) = \sum_{\mathbf{s}} \psi(\mathbf{s}, t)$. The form of Eq. (2) is a "generalized master equation" (GME) which, in contrast to Eq. (1), is non-local in time. The transition rates are stationary (i.e., depend only on the difference $\mathbf{s} - \mathbf{s}'$) and time dependent.

It is straightforward to show (Kenkre et al., 1973), using the Laplace transform, that the GME is equivalent to a CTRW

$$R(\mathbf{s},t) = \sum_{\mathbf{s}'} \int_0^t \psi(\mathbf{s} - \mathbf{s}', t - t')\, R(\mathbf{s}', t')\, \mathrm{d}t' \tag{3}$$

where $R(\mathbf{s}, t)$ is the probability per time for a walker to just arrive at site $\mathbf{s}$ at time t, and $\psi(\mathbf{s}, t)$ is the probability rate for a displacement $\mathbf{s}$ with a difference of arrival times of t. The correspondence between Eqs. (2) and (3) is detailed in Berkowitz and Scher (2000). The CTRW accounts naturally for the cumulative effects of a sequence of transitions. The challenge is to map the important aspects of the particle motion in the fracture system onto $\psi(\mathbf{s}, t)$. The identification of $\psi(\mathbf{s}, t)$ lies at the heart of the CTRW formulation.

As shown by Scher and Montroll (1975), and discussed by, e.g., Berkowitz and Scher (1998, 2000), non-Fickian transport arises in cases where the large time behavior of $\psi(\mathbf{s}, t)$ is a power law, i.e., $\psi(\mathbf{s}, t) \to t^{-1-\beta}$ for large t, for $0 < \beta < 2$. In fact, only two simple asymptotic forms of $\psi(\mathbf{s}, t)$ can exist: exponential decay and power law decay. It can be shown that exponential decay leads to Fickian transport (Margolin and Berkowitz, 2000). In the range $0 < \beta < 2$, distinctly different transport behaviors can be identified within the power law decay form. In the context of this CTRW formulation, it has been shown (Berkowitz and Scher, 1998) that "asymptotic" or "large time" behavior occurs quickly, after as few as 10 particle transitions. The relative shapes of the transport curves, and the rate of advance of the peak, vary strongly as a function of β. For $0 < \beta < 1$, transport is highly non-Fickian, and the concentration peak moves much more slowly than the Fickian, with a longer forward advance of particles. For $1 < \beta < 2$, the mean particle plume moves with the average fluid velocity, but the tails remain broader ("heavier") than those of a Fickian distribution. For $\beta > 2$, the transport becomes Fickian.

Tracer test measurements often consist of breakthrough curves of tracer concentrations as a function of time t, at selected distances from the tracer source. The breakthrough usually refers to the plane of exiting particles, and the curve corresponds therefore to an FPTD. The FPTD, denoted by $F(\mathbf{s}, t)$, is defined as the probability per time to reach site $\mathbf{s}$ at time t for the first time. The function $F(\mathbf{s}, t)$ can be determined from the implicit relation

$$R(\mathbf{s},t) = \delta_{\mathbf{s},0}\,\delta(t - 0^+) + \int_0^t F(\mathbf{s},t')\, R(0, t - t')\, \mathrm{d}t' \tag{4}$$

where $\delta_{i,j}$ is the Kronecker delta function and $\delta(t - t_0)$ is the Dirac delta function, indicating that the contaminant is at the origin at $t = 0$. To obtain a breakthrough curve, we calculate the average of the particles $\langle F(s, t)\rangle$ over the exiting boundary of the flow domain (e.g., a plane for three-dimensional systems). We do this by solving Eq. (4), following Montroll and Scher (1973) (see also Berkowitz et al., 2000), using Laplace

transforms (noting that the convolution form produces an algebraic equation for $\langle F(\mathbf{s}, u)\rangle$ in Laplace (u)-space) to obtain

$$\langle F(\mathbf{s},t)\rangle \equiv f(L,\tau) = \mathscr{L}^{-1}\{\exp(-bu^{\beta})\} \quad \text{for} \quad 0<\beta<1 \tag{5}$$

where τ is a dimensionless time (explained in Section 4.1). We define $b \equiv L/\langle l\rangle$ as the number of transitions needed for a particle to reach the exiting plane at distance L, with $\langle l\rangle$ the mean displacement length for a single particle transition.

The exact solution of Eq. (5) is

$$\tau f(\tau) \sim -\frac{1}{\pi}\sum_{j=0}^{\infty}(-x)^{j}\sin(\pi j\beta)\frac{\Gamma(j\beta+1)}{\Gamma(j+1)} \tag{6}$$

where $x = b/\tau^{\beta}$.

Numerically, we can evaluate Eq. (6) only for small to moderate values of x, because of the j exponent. For large x the $\mathscr{L}^{-1}$ expression in Eq. (5) can be approximated (Scher and Montroll, 1975) by the following equation:

$$\tau f(\tau) \sim \frac{1}{\sqrt{2\pi(1-\beta)}}(\beta x)^{\frac{1}{2(\beta-1)}}\exp\left[-\left(\frac{1-\beta}{\beta}\right)(\beta x)^{\frac{1}{1-\beta}}\right]. \tag{7}$$

Fig. 3 shows a range of cumulative FPTD curves

$$M(L,\tau) \equiv \int_0^{\tau} f(L,\tau')\mathrm{d}\tau' \tag{8}$$

vs. a dimensionless time, $\tau/b^{1/\beta}$, for a range of β values. The integrand in Eq. (8) is determined by combining Eqs. (6) and (7). As discussed in Berkowitz et al. (2000), the

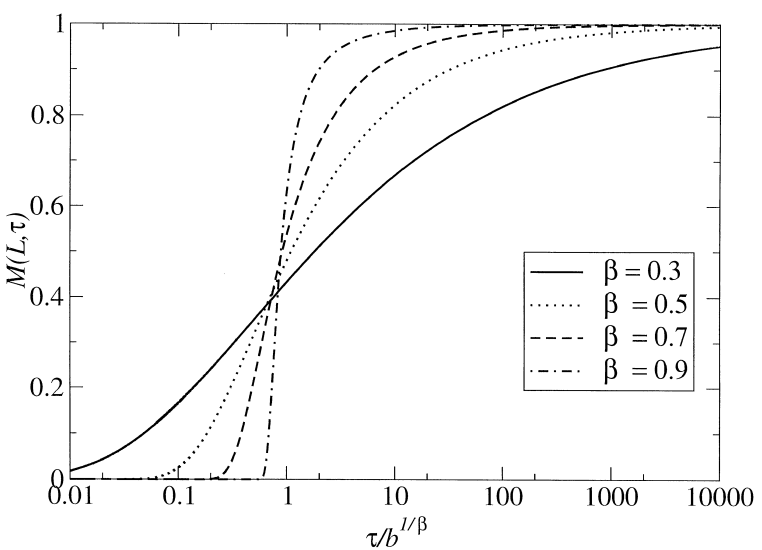

Fig. 3. Semilog plots showing a range of cumulative FPTD curves, $M(L, \tau)$, vs. the dimensionless time $\tau/b^{1/\beta}$ for $\beta = 0.3, 0.5, 0.7, 0.9$.

curves $M(L, \tau)$ in Fig. 3 are those of the typically measured normalized, cumulative concentration for step input functions. The parameters b and β are such that β controls the shape of the curve, while a change in $b^{1/\beta}$ results in a shift of $M(L, \tau)$ along the x-axis in the plots of Fig. 3. Thus, β can be considered as a "dispersion" parameter.

We stress that the low velocity regime of particle transitions determines β. Although transport of particles in fast "channels" controls the early arrival times, the bulk of the transport behavior is influenced by particles that encounter low-velocity pathways (including relatively stagnant zones in fractures and in the host rock). The shape of the curves steepens as β increases, although the front becomes steeper than Fickian and the trailing tail is longer than Fickian. The solutions and plots of breakthrough curves for $1 < \beta < 2$ are given by Margolin and Berkowitz (2000).

Non-Fickian transport can exist even in uniformly heterogeneous media on a scale much larger than the size of the heterogeneities (e.g., Berkowitz et al., 2000), so that there is a very broad length (or temporal) scale over which β is constant. Clearly, if the relative size of the heterogeneities is small at extremely large length scales — i.e., as b (the number of particle transitions between the inlet and measurement planes) becomes very large — the transport behavior becomes Fickian, with $\beta \geq 2$. For this special case, the CTRW formulation is identical to the ADE, with a scale-independent dispersion coefficient. In particular, the dispersion coefficient is determined by the limiting form of the Laplace transform of $\psi(\mathbf{s}, t)$. Additional detailed discussion of the physical and mathematical meaning of these parameters is given in Margolin and Berkowitz (2000) and Berkowitz and Scher (2000).

4. Analysis of the tracer test data

4.1. Comparison of CTRW, EPM and DFM solutions with measurements

We analyze the measured data with two different approaches: (1) treating each breakthrough curve individually and (2) analyzing flux-averaged breakthrough curves for the upper and lower samplers. As noted in the equation development, the CTRW is a fully three-dimensional formulation, and accounts for a flow field, in which contaminants are transported, that is not restricted to purely vertical flow. For comparison to the experimental data, the FPTD solutions based on the CTRW are averaged over the inlet and outlet boundary faces. Unlike the CTRW method, the forms of the EPM and DFM models used by Sidle et al. (1998) are based essentially on one-dimensional solutions of the flow and transport equations, in that they simplify the complex natural flow field to parallel flow in vertical "columns". As such, while some correlation in transport behavior can be expected between pairs of samplers in the upper and lower levels, each breakthrough curve must be treated individually. In general, of course, flow in fracture networks is three-dimensional and the flow is not necessarily predominantly downward in a single "column".

The CTRW solution Eq. (5) is based on periodic boundary conditions which, in our case, are the vertical boundaries. Periodic boundary conditions (with mass conservation)

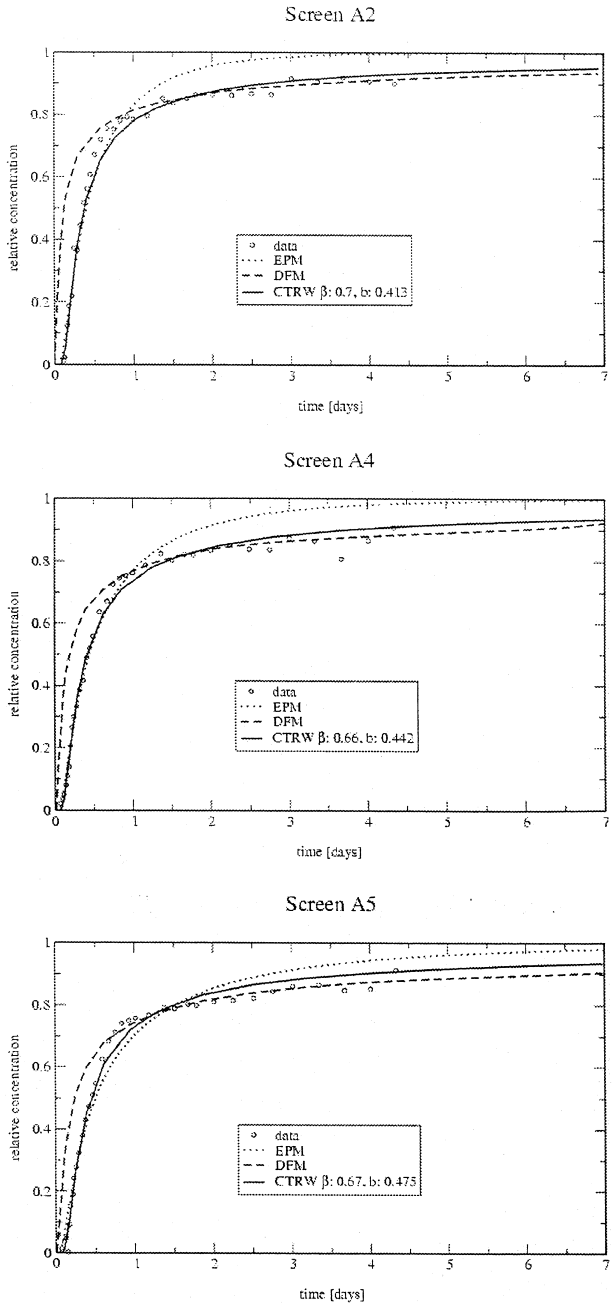

Fig. 4. Best-fit theoretical breakthrough curves based on the EPM, the DFM and the CTRW solutions. Points indicate measured values, including seven samplers at the 2.5-m depth (samplers A2–C5), and five samplers at the 4-m depth (samplers D1–F5).

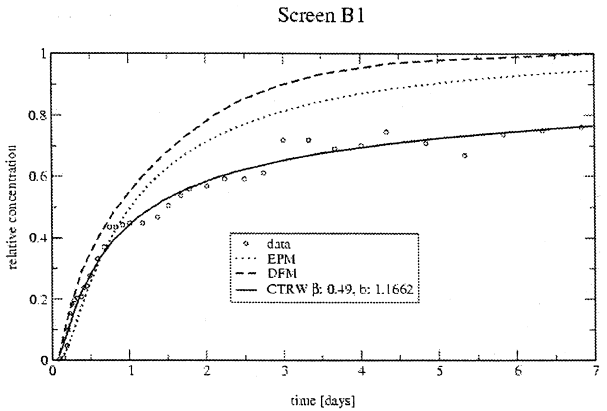

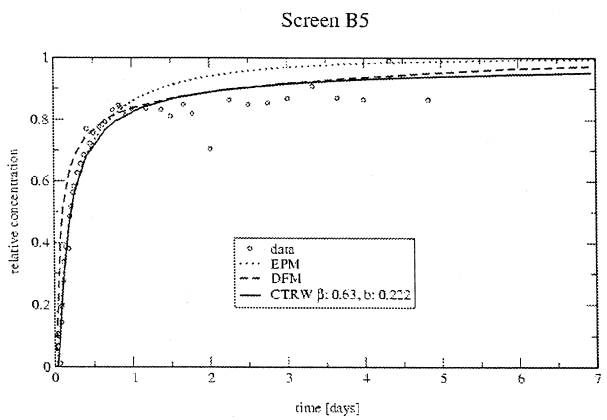

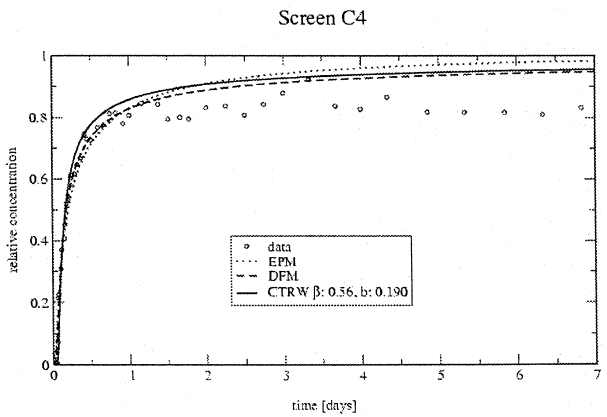

Fig. 4 (*continued*).

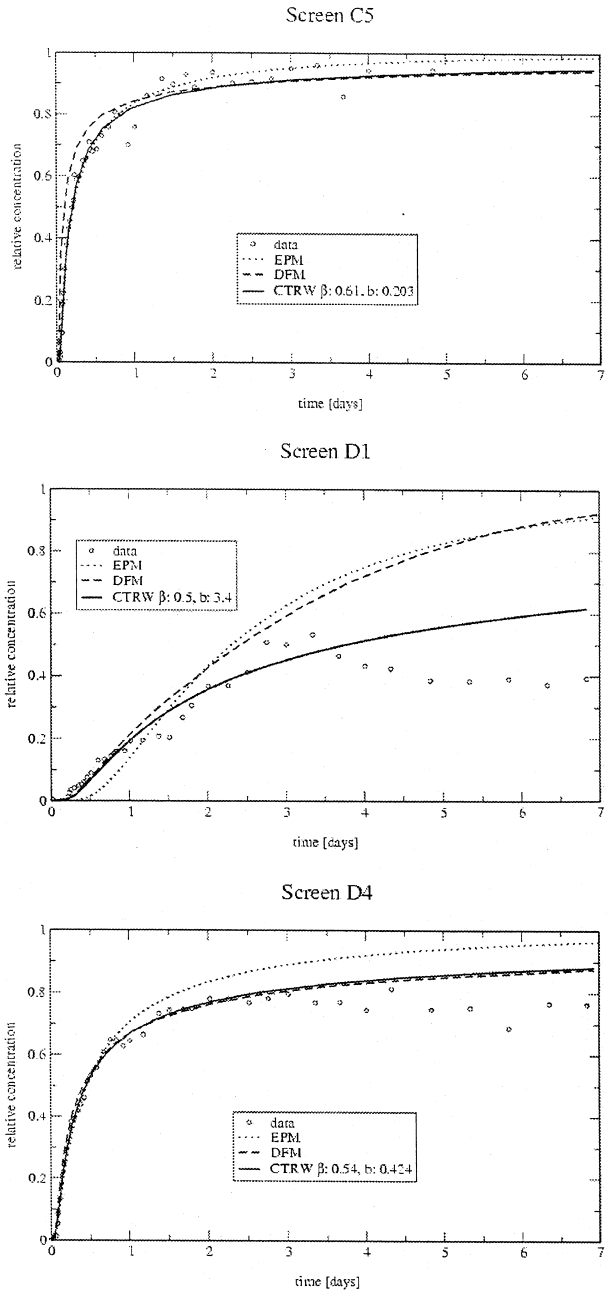

Fig. 4 (*continued*).

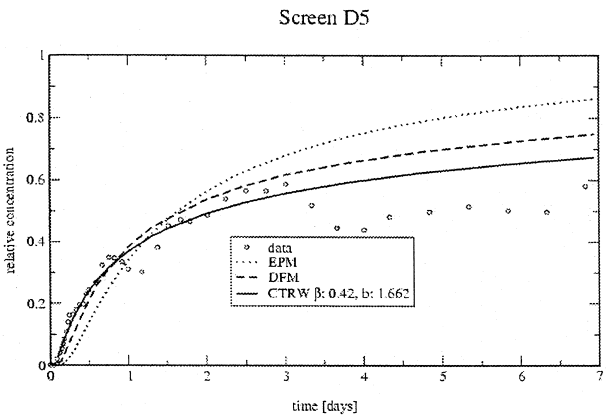

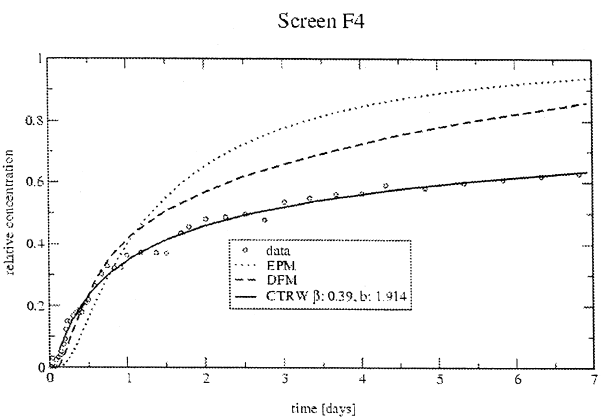

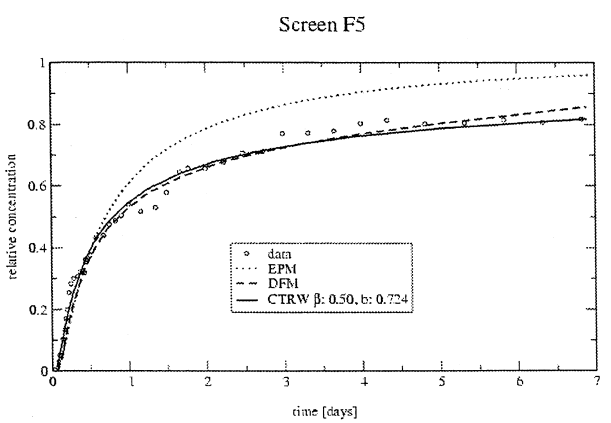

Fig. 4 (*continued*).

indeed exist in the field experiment in the sense that, statistically, all mass which leaves the domain over one vertical boundary is matched, by mass entering the domain over another vertical boundary.

As found by Sidle et al. (1998), and as shown in Fig. 4, the EPM and DFM models do not capture the full evolution (both early and late arrival times) of the tracer behavior displayed in the measured breakthrough curves. Overall, the EPM solutions fit only the early time data points, whereas the DFM solutions generally fit the late time data points. Interestingly, the flow velocities estimated by Sidle et al. (1998) for the DFM are ~ 100 times greater than those estimated for the EPM. The fitted parameters for the EPM do not appear to show any relation to the geometry of the fracture network or to the geology. With regard to the DFM, there is insufficient information available to judge the meaning of the fitted parameters. We remark also that the DFM, as applied by Sidle et al. (1998), does not account for dispersion (caused by fracture wall geometry, fracture connectivity or other deviations from the parabolic velocity profile), so that contaminant spreading is attributed only to matrix diffusion. Finally, we note that consideration of a hybrid of these two approaches would require at least four parameters to fit the data (flow velocities, dispersivity, fracture apertures and fracture separations).

Fig. 4 also shows the fit of the CTRW curves to the experimental data. We fit each experimental breakthrough curve using a separate value of β (summarized in Table 1). In general, all data points were considered when fitting the curves. Exceptions were made for breakthrough curve data from the samplers C4, D1, D4 and D5, for which only earlier times were considered. These four samplers yielded tracer concentrations which either stopped increasing, or even decreased, after about 3 days. Although no detailed information is available, such behavior might be attributed to transient variation in the hydraulic field, caused by clogging of fractures and/or changes in the inflow conditions.

The curves fit quite convincingly the measured breakthrough curves over the entire time range of the experiment. In particular, the early and late time behaviors are

Table 1
Values for best-fit breakthrough curves

Sampler	β	x_{shift}
A2	0.7	0.414
A4	0.66	0.442
A5	0.67	0.475
B1	0.49	1.166
B5	0.63	0.222
C4	0.56	0.190
C5	0.61	0.203
D1	0.5	3.400
D4	0.54	0.424
D5	0.42	1.662
F4	0.39	1.914
F5	0.5	0.724
Flux weighted average of upper samplers	0.57	0.35
Flux weighted average of lower samplers	0.40	1.24

Samplers A2–C5 lie at the 2.5-m depth, while samplers D1–F5 lie at the 4-m depth.

captured remarkably well. We emphasize that the characteristic information, which distinguishes non-Fickian transport from Fickian transport — as embodied either explicitly or implicitly, e.g., in the EPM and DFM models — in fact lies in the early and late arrival times of the breakthrough curves.

As seen in Table 1, the β values that fit the breakthrough curves (all of which are significantly smaller than unity) lie in a relatively narrow range. In the context of this field experiment, variation in β values is expected because of the discrete nature of the fracture system. At least some of the fluid and tracer movement is restricted to poorly connected fracture and discrete flow paths. Significantly, variations in the controlling "dispersion" parameter β are clearly locally correlated to the physical characteristics of the system. Smaller values of β are typical of more dispersive (heterogeneous) systems (recall Fig. 3). Here, the values of β are in general higher for the upper samplers ($\beta = 0.49–0.7$) than for the lower samplers ($\beta = 0.39–0.54$). In particular, compare the β values (Table 1) for the pairs of samplers which have the same horizontal position but different depths (A4–D4, A5–D5, C4–F4, C5–F5; see Fig. 1): β is consistently smaller at the lower samplers. This indicates that as the tracer travels over longer distances, the apparent degree of overall heterogeneity in the flow field increases. This result is consistent with the geological mapping which indicates that fracturing becomes sparser with depth (see Section 2), and our treatment of the system as a series of quasi-one-dimensional (vertical) columns. We examine this treatment further in Section 4.2.

Fig. 5 shows CTRW fits on averaged concentration data sets. The convolution curve fit for the lower samplers will be discussed below in Section 4.2.1. We calculated the concentration points by taking the weighted average of concentrations in all upper samplers (and all lower samplers) for each time. We used the volumetric flow rate towards each sampler as the individual weights, which were calculated from the mass flux and the cross-sectional capture area for each sampler (data from Table 1 of Sidle et al., 1998). Some late time data points for the upper samplers were excluded from our analysis, because the averages of these data points were based only on data from two samplers.

The fits in Fig. 5 are also remarkably good. As for the single breakthrough curves, the value for β is higher for the upper samplers (0.57) than for the lower samplers (0.4). Moreover, both values of β lie in the lower ranges of β found for the respective single sets of curves.

As mentioned above, while β reflects the degree of heterogeneity, fitting of the FPTD curves to the experimental data also involves estimation of a "shift factor" x_{shift}, which translates the FTPD curve along the time (x) axis. Clearly, both x_{shift} and β may vary among the quasi-one-dimensional columns. To analyze the x_{shift}, we apply a procedure similar to Berkowitz et al. (2000); we translate the theoretical breakthrough curve along the x-axis by multiplying the dimensionless quantity $\tau/b^{1/\beta}$ by x_{shift}.

We start with the definition of the dimensionless time $\tau \equiv \bar{v}t/\langle l \rangle$, where t is the experiment time and $\bar{v}$ is a characteristic flow velocity for the particle transitions. The value of $\bar{v}$ is larger than that of the average fluid velocity in the domain. We recall that $b \equiv L/\langle l \rangle$, where L is the distance between the inflow boundary and the measurement plane and $\langle l \rangle$ is the mean displacement for a single transition. Comparing the time at which $C/C_0 = 0.5$ on a breakthrough curve fit with a value of β, we denote by B' the

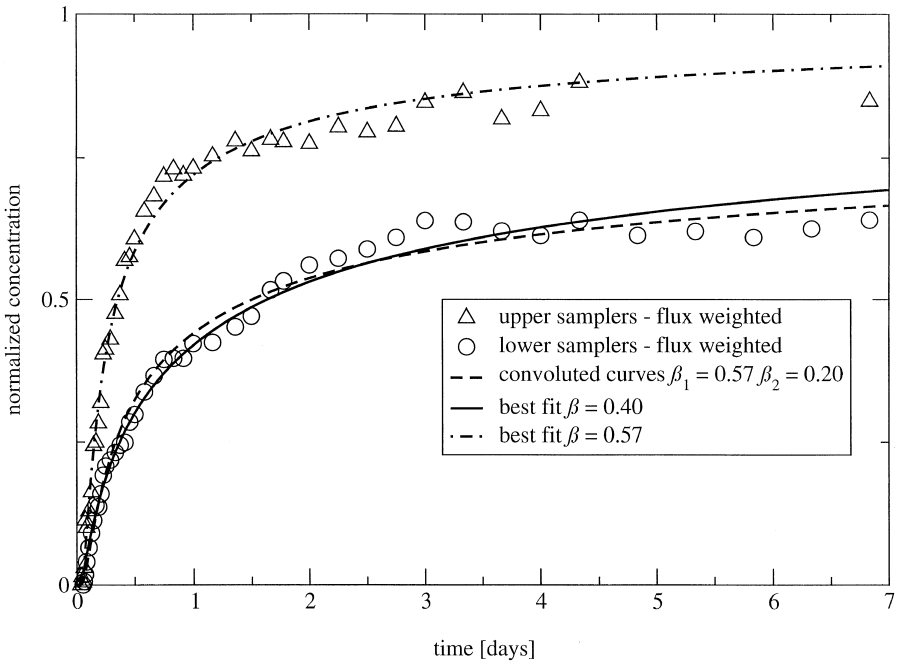

Fig. 5. Best-fit theoretical breakthrough curves based on the CTRW solutions. Triangles and circles indicate the flux-weighted averages of the measured breakthrough data for the upper and lower samplers. For the lower samplers, a fit based on the convolution of two CTRW solutions with different β is also shown.

value of $\tau/b^{1/\beta}$, at which $C/C_0 = 0.5$. Thus, the dimensional (experiment) time at which $C/C_0 = 0.5$ is

$$t = \frac{B'\langle l\rangle}{\bar{v}}\left(\frac{L}{\langle l\rangle}\right)^{1/\beta}. \tag{9}$$

From Eq. (9), we can easily extract x_{shift}, because $t = B' x_{\text{shift}}$:

$$x_{\text{shift}} = \frac{\langle l\rangle}{\bar{v}}\left(\frac{L}{\langle l\rangle}\right)^{1/\beta}. \tag{10}$$

Unlike the heterogeneous system studied by Berkowitz et al. (2000), the mean size of the low permeability heterogeneities in the field site is not particularly well-defined. In principle, information on the relative sizes of the heterogeneities can be used to estimate $\langle l\rangle$. Then from Eqs. (9) or (10), the characteristic velocity $\bar{v}$ can be estimated. In the absence of well-defined estimates, we chose here simply to determine the value of the shift factor that yielded the best fit to each measured breakthrough curve. It is important to stress that there is some interplay, or flexibility, in the choice of $\bar{v}$ and $\langle l\rangle$. Thus, we verified that the shift factor values appearing in Table 1 are consistent with the actual flow domain — for each of the shift factor values, we used Eq. (9) to estimate values of $\bar{v}$ and $\langle l\rangle$. A sensitivity analysis showed that values of $\langle l\rangle$ can thus be estimated to lie

in the range of 0.1–1.0 m; these values are entirely consistent with the expected scale of heterogeneity evident at the field site.

Once a measured breakthrough curve is fitted and the values for β and x_{shift} for a fixed transport distance L are known, predictions for the breakthrough behavior at other transport distances are possible. This application assumes, similar to the EPM and DFM approaches, that the degree of heterogeneity is not changing over the length scale of our transport problem. In this case only L is variable in Eq. (10) and the new x_{shift} can be calculated easily.

4.2. Convolution solutions using the CTRW model

We described in Section 3 how to calculate the spatial and temporal evolution of an input function in the form of a δ-pulse or a step function. In many experimental systems, especially at the field scale, it can be difficult to realize these initial conditions exactly. It is, however, straightforward to use convolution techniques to account for other boundary conditions. Convolutions can also be used to account for transport through different regions (layers) with different properties (i.e., different β values).

4.2.1. Convolution theory

For the calculation of breakthrough curves for input functions of any form, we convolute the input function $F(t)$ with the function $G(t)$, where $G(t)$ is the response function for the medium, corresponding to the function for the FTPD of a pulse input. The convolution of $F(t)$ and $G(t)$ is defined as

$$H = F(t)G(t) = \int_0^t F(t-\tau)G(\tau)\mathrm{d}\tau. \tag{11}$$

Fig. 6 shows schematically applications of the convolution relevant to experimental conditions considered here. These cases illustrate convolutions of breakthrough curves from $F(t)$, for a specific β, with another function $G(t)$ having a different β. The resulting convolutions in these two cases correspond to breakthrough curves arising for a system where the tracer is transported through two layers with different β values. Alternatively, these figures illustrate input functions for the typical cases of "near-step" inputs, convoluted with $G(t)$ having a specific β. Two special cases are not shown in Fig. 6: if $F(t)$ is an exact δ-pulse, the convolution with $G(t)$ simply reproduces $G(t)$, while if $F(t)$ is an exact step function the convolution with $G(t)$ yields a cumulative breakthrough curve.

4.2.2. Two regions with different transport behavior

Sidle et al. (1998) discuss the apparent existence of two different layers in the field site — a highly connected upper domain and a lower domain dominated by flow in single fractures (although, as already noted, the hydraulic properties of these layers are not known). In the CTRW framework, the value of β in the upper domain could be expected to be higher than in the lower domain, because the transport may be more "homogeneous". Thus, the breakthrough curve measured in the second layer can be treated with the CTRW approach by using a convolution of two breakthrough curves

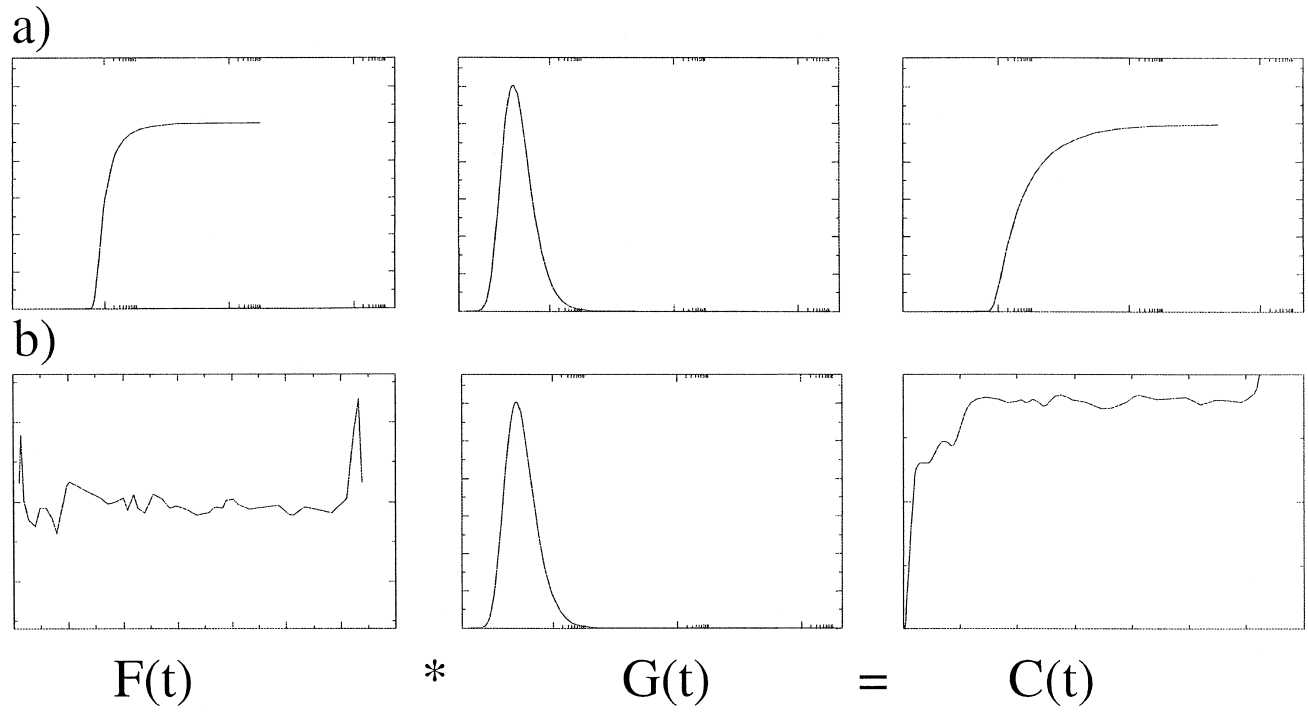

Fig. 6. Schematic illustrations of convolutions of functions $F(t)$ and $G(t)$, each having a different β, and the resulting breakthrough curves $C(t)$. Panels (a) and (b) show respectively, input functions for the typical cases of "near-δ-pulse" and "near-step" inputs, convoluted with $G(t)$ having a specific β.

Table 2
Values for best-fit convoluted breakthrough curves

Sampler	β	x_{shift}
D5	0.19	0.04
F4	0.32	0.7
F5	0.41	0.16
Flux weighted average of lower samplers	0.20	0.035

based on β values in the upper and lower layers, β_1 and β_2. In other words, in the context of the field experiment discussed here, the breakthrough curve for the upper sampler can be used as an input function for the lower sampler. Thus, we convolute the known breakthrough curve for the upper sampler and with an unknown FPTD for the lower sampler.

The β values and factors for shifting along the x-axis for the fits with two convoluted curves are summarized in Table 2. In Figs. 5 and 7 we show fits of the averaged data points for the lower samplers obtained by a convoluted breakthrough curve with different β_1, β_2 values, compared to a breakthrough curve with a single β. The lognormal time axis in Fig. 7 allows the more detailed analysis of the early arrival times. The early time behavior of the convoluted curve is similar to the curve with

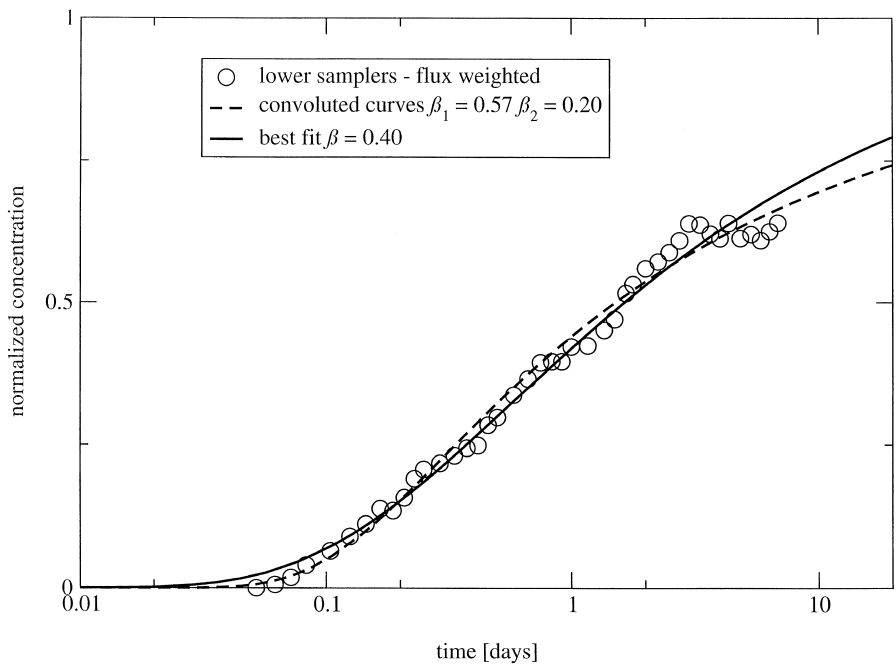

Fig. 7. Semilog plot of the flux-weighted averaged breakthrough data for the lower sampler. Also shown are the best-fit CTRW solution and a fit based on the convolution of two CTRW solutions.

greater β (i.e., the curve has a steep slope), whereas the late time behavior is dominated by the curve with lower β (longer tailing). Of course, for the field experiment discussed here, the uncertainty and lack of information make it difficult to distinguish between the quality of the different fits. The fit with the convoluted breakthrough curve is remarkably good for the early times. For intermediate and greater times, the breakthrough curve for a single β seems more appropriate. The low value of β for the lower region corresponds to a lower fracture density. The transport in this lower region could be dominated by a relatively small number of fractures intersecting the domain, and the non-Fickian transport could be due to excursions through the rough wall topology of the fractures. In any case, the two values of β relate well to the apparent hydraulic differences between the regions.

5. Concluding remarks

The tracer breakthrough data presented by Sidle et al. (1998) display behavior that is characteristic of non-Fickian transport. The conventional EPM and DFM models clearly fail to describe and explain the measured breakthrough curves. Application of more sophisticated multi-parameter or stochastic models is predicated on being able to demonstrate that these models are physically based, valid over all relevant scales, and effective without additional knowledge about the system.

We have analyzed this data set with a CTRW approach, which is based on a physical picture of contaminant motion that is consistent with the geometric and hydraulic characterization of the fractured formation. The limitations in the experimental set-up, the uncertain knowledge of the hydraulic properties of the domain, and the low resolution of the measurements permit study of the nature of the tracer transport, rather than analysis of modeling approaches in a predictive framework. Additional experiments are necessary to more fully examine the predictive capacity of the CTRW theory and other approaches.

The entire shape of the FPTD solutions are characterized by the “dispersion” parameter β. The value of β is controlled by the degree of heterogeneity of the hydraulic conductivity field, which in turn essentially controls the velocity distribution; it is straightforward to estimate β directly from the velocity distribution, if it is available. Thus, β is a measurable, physically based parameter and replaces the standard dispersion coefficient which relates only to the second moment of the plume. Sidle et al. (1998) and Klint and Fredericia (1995) found a decreasing fracture intensity and connectivity with depth, which is reflected in the lower values of β at greater depth.

Fitting of the FPTD solutions to breakthrough measurements also requires knowledge of the mean size of the local heterogeneities, in order to estimate the mean displacement for a single transition, $\langle l \rangle$. Only weak knowledge of the local heterogeneities is available at the field site. However, our estimates of $\langle l \rangle$ (and thus of the characteristic velocity $\bar{v}$) are entirely consistent with the available information. Alternatively, another approach would be to estimate $\bar{v}$ (based on the velocity distribution); but this is generally more difficult than measuring the geometry.

The CTRW framework captures quantitatively a broad range of non-Fickian and Fickian transport behaviors, and can be used in a predictive capacity. The solutions are robust, and require a minimum number of fitting parameters. These parameters can be estimated on the basis of one or more measured breakthrough curves, and/or on the basis of information on the distribution of the velocity field and the relative scale of heterogeneity. Moreover, we have shown how convolution techniques can be used to obtain solutions for breakthrough behavior of tracer that migrates through regions with different dispersive properties and general input flow conditions. Generalization of these ideas for application to large-scale aquifer systems is currently under development.

Acknowledgements

We appreciate the assistance of Bertel Nilsson, who generously supplied us with the data from the field experiment. The financial support of the European Commission (Contract No. ENV4-CT97-0456) is gratefully acknowledged. The authors thank the two anonymous reviewers for useful comments.

References

Adams, E.E., Gelhar, L.W., 1992. Field study of dispersion in a heterogeneous aquifer: 2. Spatial moment analysis. Water Resour. Res. 28 (12), 3293–3308.

Berkowitz, B., Scher, H., 1995. On characterization of anomalous dispersion in porous and fractured media. Water Resour. Res. 31 (6), 1461–1466.

Berkowitz, B., Scher, H., 1997. Anomalous transport in random fracture networks. Phys. Rev. Lett. 79 (20), 4038–4041.

Berkowitz, B., Scher, H., 1998. Theory of anomalous chemical transport in fracture networks. Phys. Rev. E 57 (5), 5858–5869.

Berkowitz, B., Scher, H., 2000. The role of probabilistic approaches to transport theory in heterogeneous media. Transp. Porous Media, in press.

Berkowitz, B., Scher, H., Silliman, S.E., 2000. Anomalous transport in laboratory-scale, heterogeneous porous media. Water Resour. Res. 36 (1), 149–158.

Broholm, K., Nilsson, B., Sidle, R.C., Arvin, E., 2000. Transport and biodegradation of creosote compounds in clayey till, a field experiment. J. Contam. Hydrol. 41, 239–260.

Eggleston, J.R., Rojstaczer, S., 1998. Identification of hydraulic conductivity trends and the influence of trends on contaminant transport. Water Resour. Res. 34 (9), 2155–2168.

Fitts, C.R., 1996. Uncertainty in deterministic groundwater transport models due to the assumption of macrodispersive mixing: evidence from the Cape Cod (Massachusetts, USA) and Borden (Ontario, Canada) tracer tests. J. Contam. Hydrol. 23, 69–84.

Hatano, Y., Hatano, N., 1998. Dispersive transport of ions in column experiments: an explanation of long-tailed profiles. Water Resour. Res. 34 (5), 1027–1033.

Kenkre, V.M., Montroll, E.W., Shlesinger, M.F., 1973. Generalized master equations for continuous-time random walks. J. Stat. Phys. 9 (1), 45–50.

Klafter, J., Silbey, R., 1980. Derivation of continuous-time random-walk equations. Phys. Rev. Lett. 44 (2), 55–58.

Klint, K.E., Fredericia, J., 1995. Sprækeparametre i moæneler. Vand Jord 2 (5), 208–214.

Margolin, G., Berkowitz, B., 2000. Application of continuous time random walks to transport in porous media. J. Phys. Chem. 104 (16), 3942–3947.

Montroll, E.W., Scher, H., 1973. Random walks on lattices: IV. Continuous-time walks and influence of absorbing boundaries. J. Stat. Phys. 9 (2), 101–135.

National Research Council, 1996. Rock Fractures and Fluid Flow: Contemporary Understanding and Applications. National Academy Press, Washington, DC.

Ogata, A., Banks, R.B., 1961. A solution of the differential equation of longitudinal dispersion in porous media. U.S. Geol. Surv. Prof. Pap. 411-I.

Oppenheim, I., Shuler, K.E., Weiss, G.H., 1977. The Master Equation. MIT Press, Cambridge.

Sahimi, M., 1995. Flow and Transport in Porous Media and Fractured Rock. VCH Verlagsgesellschaft, Weinheim.

Scher, H., Lax, M., 1973a. Stochastic transport in a disordered solid: I. Theory. Phys. Rev. B 7 (10), 4491–4502.

Scher, H., Lax, M., 1973b. Stochastic transport in a disordered solid: II. Impurity conduction. Phys. Rev. B 7 (10), 4502–4519.

Scher, H., Montroll, E.W., 1975. Anomalous transit-time dispersion in amorphous solids. Phys. Rev. B 12 (6), 2455–2477.

Shlesinger, M.F., 1996. Random processes. Encyclopedia of Applied Physics vol. 16. VCH Publishers, New York.

Sidle, C.R., Nilsson, B., Hansen, M., Fredericia, J., 1998. Spatially varying hydraulic and solute transport characteristics of a fractured till determined by field tracer tests, Funen, Denmark. Water Resour. Res. 34 (10), 2515–2527.